6

Effects of Ionizing Radiation on Optoelectronic Devices

V. Th. Tsakiri[1], A. P. Skountzos[1], P. H. Yannakopoulos[1] and E. Verrelli[2]
[1]*TEI Piraeus – P.Ralli and Thivon 250, 12244 Aigaleo, Attica,*
[2]*National Technical University of Athens, Dept. of Applied Physics,*
Zografou Campus, 15780
Greece

1. Introduction

The devices, whose function is based on the interaction of electronic processes with either light or optical processes, are called optoelectronic devices. This interaction is usually accompanied by an energy conversion process (such as electrical to optical and vice versa). Optoelectronic devices are made from semiconducting materials. Research and development of optoelectronic devices and optoelectronic integrated circuits have received a tremendous boost with the development of low-loss optical fibers for long distance communication and the development of new immune to radiation optoelectronic devices used in the aerospace industry. In the following paragraphs we describe the semiconductor materials used in optoelectronic applications in combination with the electromagnetic theory. We focused on the OLEDs and IRLEDs and we present some of the SRIM –TRIM and CASINO simulation results.

2. Optoelectronic devices

2.1 Semiconductor materials

The elemental semiconductors, especially Si, which is proved to be very useful for microelectronics, have some important drawbacks. Their band gap is indirect, resulting in poor light emission and low absorption coefficients. On the other hand compound semiconductor materials offered many of the desired properties and could be synthesized relatively easy. These materials are made from elements of different columns of the periodic table resulting in III-V, II-VI or IV-IV compounds. III-V compounds have been the first and most widely used semiconducting materials

Before referring to the advantages of some characteristic compounds, we should point out the structural difference between direct and indirect semiconductors. The top of the valence band of most semiconductors occurs at a value of effective momentum (k), equal to zero. Semiconductors in which the bottom of the conduction band is also at $k = 0$ are direct band gap materials. Semiconductors in which the bottom of the conduction band occurs at other points in momentum space are indirect band gap materials. According to the atomic structure of the semiconductors, their outermost valence electrons are in s- or p-type

orbitals. Although true only for elements in their atomic form, the s- or p-like character is also retained in the crystalline semiconductors. The bands of a semiconductor are a result of the crystal potential that originates from the equilibrium arrangement of atoms in the lattice. If the edge of the conduction band is made up of s-type states, the semiconductor is direct band gap. If, on the other hand, the lowest conduction band edge is made up of p-type states, then the semiconductor is indirect band gap.

One characteristic example of semiconductor compound is indium antimonite (InSb), the first to be discovered in 1950, presenting low bandgap, E_g = 0.17 eV, and consequently applied in far infrared detector technology. Moreover, the invention of the semiconductor laser and the discovery of the Gunn Effect, turned the interest to other III-V compounds such as GaAs *(E_g* = 1.43 eV) and InP *(E_g* = 1.35 eV). GaP, which has its band gap (E_g = 2.1 eV) in the visible part of the spectrum is important for the development of the light-emitting diode (LED). GaP band gap is indirect, but by certain doping techniques, the radiative efficiency can be improved.

One main advantage of the Binary compounds is that they can be combined or "alloyed" to form Ternary or Quaternary compounds. These compounds are made up of three or four group III and group V atoms and, by choosing different elements it is possible to create materials of different band gaps, with various emission energies for light sources. However, by alloying, it is possible to vary the band gap continuously and monotonically and together with it, the band structure and the electronic and optical properties. The varying band gap also allows the building of heterojunctions, which are important for high-performance electronic and optoelectronic devices. The quaternary compounds of $In_xGa_yAl_{1-x-y}As$, and $In_{1-x}Ga_xAs_yP_{1-y}$ present band gaps which correspond to the spectral window in which silica fibers have their lowest loss and dispersion, making their research and development very important for optical communications. (Bhattacharya, 1997)

2.2 Electron – hole formation and recombination

The creation or annihilation of electron-hole pairs rules the operation of almost all optoelectronic devices. Pair formation involves raising an electron in energy from the valence band to the conduction band, resulting with a hole behind in the valence band. In principle, any energetic particle incident on a semiconductor, which can impart energy at least equal to the bandgap energy to a valence band electron, will create pairs. The simplest way to create electron-hole pairs is to irradiate the semiconductor. Photons with sufficient energy are absorbed, and these impart their energy to the valence band electrons raising them to the conduction band. This process is, therefore, also called absorption. The reverse process, that of electron and hole recombination, is associated with the pair giving up its excess energy after recombination. This process may be radiative or non-radiative. In a non radiative transition, the excess energy due to recombination is usually imparted to phonons and dissipated as heat in the material. In a radiative transition, the excess energy is dissipated as photons, usually having energy equal to the bandgap. This is the luminescent process, which is classified in three cases according to the method by which the electron-hole pairs are created: a) Photoluminescence, involves the radiative recombination of electron-hole pairs created by injection of photons, b) cathodoluminescence, involves radiative recombination of electron-hole pairs created by electron bombardment and c) electroluminescence, involves radiative recombination following carriers' injection in a p-n junction.

In the case of a semiconductor in equilibrium (i.e., without any incident photons or injection of electrons), the carrier densities can be calculated from an equilibrium Fermi level using Fermi-Dirac or Boltzmann statistics. When excess carriers are created by one of the techniques described above, non-equilibrium conditions are generated and the concept of a Fermi level is no longer valid. One can, however, define non-equilibrium distribution functions for electrons and holes as:

$$f_n(E) = \frac{1}{1+\exp\left(\frac{E-E_{fn}}{k_\beta T}\right)} \tag{1}$$

$$1 - f_p(E) = \frac{1}{1+\exp\left(\frac{E-E_{fp}}{k_\beta T}\right)} \tag{2}$$

where E_{fn} and E_{fp} are the quasi-Fermi levels for electrons and holes respectively. For the non-degenerate case (the Fermi level is several kT below E_c), the distribution functions of equations 1, 2 can be written as:

$$f_n(E) \cong \exp\left(\frac{E_{fn}-E}{k_\beta T}\right) \tag{3}$$

$$f_p(E) \cong \exp\left(\frac{E-E_{fp}}{k_\beta T}\right) \tag{4}$$

and the non-equilibrium carrier concentrations are given by:

$$n = N_c \exp\left(\frac{E_{fn}-E_c}{k_\beta T}\right) \tag{5}$$

$$p = N_v \exp\left(\frac{E_v-E_{fp}}{k_\beta T}\right) \tag{6}$$

The quasi-Fermi levels, provide the proper tool for calculating the changes of carrier concentration as a function of position in a semiconductor.

Generation and recombination processes involve transition of electrons across the energy bandgap and differ for direct and indirect bandgap semiconductors. In a direct bandgap semiconductor, the valence band maximum and the conduction band minimum occur at the zone center (k = 0) so that by an upward or downward transition of electrons the momentum is conserved. Therefore, in direct bandgap semiconductors such as GaAs, an electron raised to the conduction band, (i.e. by photon absorption) will dwell there for a very short time and recombine again with a valence band hole to emit light of energy equal

to the bandgap. In the case of an indirect bandgap semiconductor, where the conduction band minima are not at $k = 0$, upward or downward transition of carriers results in a momentum change so that the involvement of a phonon is needed for the conservation of momentum. Thus, an electron dwelling in the conduction band minimum, cannot recombine with a hole at $k = 0$ until a phonon with the right energy and momentum is available. Both phonon emission and absorption processes can assist the downward transition. In order for the right phonon collision to occur, the dwell time of the electron in the conduction band increases. Consequently the probability of radiative recombination is much higher in direct than indirect bandgap semiconductors justifying the use of them as light sources such as light-emitting diodes and lasers.
Moreover impurities and defects in the crystal lattice also serve as traps and recombination centers. It is most likely that an electron and a hole recombine non-radiatively through such a defect center and the excess energy is dissipated into the lattice as heat. As advanced epitaxial techniques are being developed, the purity of the crystals continues to improve. The simulation that is presented aims in the investigation of the defects generated under ionized radiation. .(Bhattacharya, 2003)

2.3 Radiative and non-radiative recombination

For continuous carrier generation by optical excitation or injection, a quasi-equilibrium or steady state is produced. Electrons and holes are created and annihilated in pairs and, depending on the injection level, a steady-state excess density is established in the crystal, also necessary for the overall charge neutrality. When the excitation source is removed, the density of excess carriers returns to the equilibrium values, n_0 and p_0. The excess carriers usually decay exponentially with respect to time following the -exp (-t/r), where *r* is defined as the lifetime of excess carriers. The lifetime is determined by a combination of intrinsic and extrinsic parameters, and affects the performance characteristics of most optoelectronic devices. It should be noted that, depending on the semiconductor sample and its surface, there can be a very strong surface recombination component which depends on the density of surface states.
Generally, the excess carriers decay by radiative and/or non-radiative recombination, in which the excess energy is dissipated by photons and phonons. The former is of importance for the operation of luminescent devices. Non-radiative recombination usually takes place via surface or bulk defects and traps and reduces the radiative efficiency of the material. Consequently the research in materials aims in reducing these non-radiative centers by optimizing the fabrication method or by applying passivation techniques on these centers.

2.4 Electromagnetic description of reflection and refraction

The function and the properties of the materials used in optoelectronic devices are strongly determined by the propagation of plane, single-frequency, electromagnetic waves. By the Maxwell's equations, useful expressions can be obtained for the dissipation, storage and transport of energy, resulting from the propagation of waves in material media. Moreover analyzing the incidence, reflection and transition of an electromagnetic wave on the border surface between two dielectric materials, can result in a better comprehension of optoelectronic devices.

2.4.1 Maxwell's equations

The following four laws constitute the basis for the electromagnetic theory:

Gauss's law for electric fields: $$\vec{\nabla} \circ \vec{E} = \rho / \varepsilon_0 \quad (7)$$

Gauss's law for magnetic fields: $$\vec{\nabla} \circ \vec{B} = 0 \quad (8)$$

Faraday's law: $$\vec{\nabla} \times \vec{E} = -\frac{\partial \vec{B}}{\partial t} \quad (9)$$

Ampere – Maxwell law: $$\vec{\nabla} \times \vec{B} = \mu_0 \left(\vec{J} + \varepsilon_0 \frac{\partial \vec{E}}{\partial t} \right) \quad (10)$$

The laws above can be applied in combination with the constitutive equations:

$$\vec{D} = \varepsilon_0 \vec{E} + \vec{P} \text{ and } \vec{B} = \mu_0 \left(\vec{H} + \vec{M} \right) \quad (11)$$

where J, is the current density, E and H are the electric and magnetic fields respectively, D and B, are the electric and magnetic displacements and P and M, are the electric and magnetic polarizations respectively.

Considering that in the dielectric materials there are no free charge carriers and currents, the application of Maxwell's equations, in combination with the constitutive equations result in the boundary conditions standing at the boundary surface between two dielectric materials. These conditions denote that during the transition from the dielectric 1 to the dielectric 2, the tangential (at the boundary surface) components of E and H as well as the normal (at the boundary surface) components of D and B, are continuous. The mathematical expression can be written as follows:

$$E_{2t} = E_{1t}, \quad H_{2t} = H_{1t}, \quad D_{2n} = D_{1n} \quad \text{and} \quad B_{2n} = B_{1n}$$

where the indexes 1 and 2 denote the limiting values, in the case of approaching the boundary surface from the dielectric 1 or 2.

These boundary conditions will serve for the calculation of important coefficients in the case of reflection and transmission of light. (Yariv,1976)

2.4.2 Reflection and refraction

2.4.2.1 Angle of incidence = 0°

In figure 1, the vectors of the electric (**E**) and magnetic (**H**) fields are subscripted as "i" for incident wave, "r" for reflected wave and "t" for transmitted wave. In this case the respective equations in complex form, for the vectors of the fields E(electric) and H(magnetic) will be:

$$\begin{aligned} E_{iy} &= E_{i0} e^{i(\omega t - k_1 x)} \quad H_{iz} = H_{i0} e^{i(\omega t - k_1 x)} \quad (x \prec 0) \\ E_{ry} &= E_{r0} e^{i(\omega t - k_1 x)} \quad H_{rz} = H_{r0} e^{i(\omega t - k_1 x)} \quad (x \prec 0) \\ E_{ty} &= E_{t0} e^{i(\omega t - k_2 x)} \quad H_{tz} = H_{t0} e^{i(\omega t - k_2 x)} \quad (x \succ 0) \end{aligned} \quad (12)$$

In the above equations, the unknown quantities are the amplitudes: E_{r0} and E_{t0}. By these, are defined the coefficient of reflection $r=E_{r0}/E_{i0}$ and the coefficient of transmission $t=E_{t0}/E_{i0}$. These coefficients can be calculated by applying boundary conditions for the fields E and H, and finally the quantities of E_{r0} and E_{t0} can be calculated. Finally:

$$r = \frac{n_1\mu_2 - n_2\mu_2}{n_1\mu_2 + n_2\mu_1} \tag{13}$$

and

$$t = \frac{2n_1\mu_2}{n_1\mu_2 + n_2\mu_1} \tag{14}$$

where $n_{1,2}$ and $\mu_{1,2}$ are the refraction coefficient and magnetic permeability respectively, of the two dielectric materials. (Papakitsos,2002)

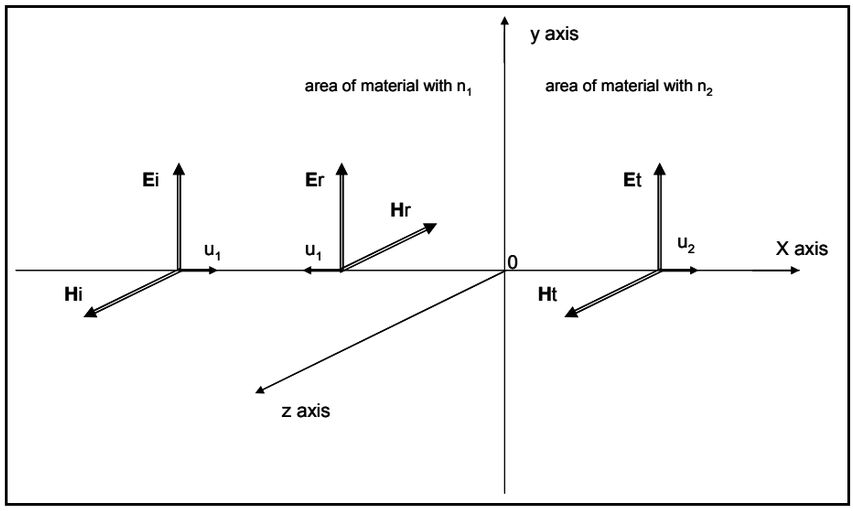

Fig. 1. EMF vectors presenting the transmission and reflection of an EM wave incident at a boundary surface between to dielectric materials

By the coefficients above, also the quantities of reflectance, R and transmittance, T can be calculated. These quantities are defined as: $R = \frac{I_r}{I_i}$ and $T = \frac{I_t}{I_i}$ where I_r is the intensity of the reflected wave, I_i is the intensity of the incident wave and I_t is the intensity of the transmitted wave. In the special case of angle of incidence = 0^o,

$$R = \frac{n_1 |E_{r0}|^2 / 2c\mu_1}{n_1 |E_{i0}|^2 / 2c\mu_1} = \left|\frac{E_{r0}}{E_{i0}}\right|^2 = |r|^2 \tag{15}$$

and

$$T = \frac{n_2 |E_{t0}|^2 / 2c\mu_2}{n_1 |E_{r0}|^2 / 2c\mu_1} = \frac{n_2\mu_1}{n_1\mu_2}\left|\frac{E_{t0}}{E_{r0}}\right|^2 = \frac{n_2\mu_1}{n_1\mu_2}|t|^2 \tag{16}$$

From the above relations, the energy conservation is proved, since R+T=1!

In the case of transparent dielectrics, where the magnetic permeability is semi equal to the magnetic permeability of vacuum, the above relations are far simplified as follows:

$$r = \frac{n_1 - n_2}{n_1 + n_2},\ t = \frac{2n_1}{n_1 + n_2},\ R = \left(\frac{n_1 - n_2}{n_1 + n_2}\right)^2 \text{ and } T = \frac{4n_1 n_2}{\left(n_1 + n_2\right)^2}$$

It is important to note that $r = \begin{cases} \succ 0 & for \quad n_1 \succ n_2 \\ \prec 0 & for \quad n_1 \prec n_2 \end{cases}$ but $t \succ 0$ for every n_1, n_2.

The physical meaning hiding here is that when a wave is heading from a material with n_1 to a material with n_2 with $n_1 \succ n_2$ the phase of the reflected wave is unchanged in accordance to the phase of the incident wave. On the opposite case ($n_1 \prec n_2$) the phase of the reflected wave has a difference of π in accordance to the phase of the incident wave.

2.4.2.2 Angle of incidence = θ°

In the case of a random angle of incidence, we consider the transverse wave of the electric field (TE) and the transverse wave of the magnetic field (TM). Consequently, following the method of figure 1, the coefficients r and t are now written as:

For the transverse wave of the electric field $r_E = \frac{E_{r0}^E}{E_{i0}^E},\ t_E = \frac{E_{t0}^E}{E_{i0}^E}$ and

for the transverse wave of the magnetic field $r_M = \frac{E_{r0}^M}{E_{i0}^M},\ t_M = \frac{E_{t0}^M}{E_{i0}^M}$.

By applying again the boundary conditions for the fields, the coefficients r and t can be calculated:

$$r_E = \frac{\cos\theta - \sqrt{n^2 - \sin^2\theta}}{\cos\theta + \sqrt{n^2 - \sin^2\theta}},\ t_E = \frac{2\cos\theta}{\cos\theta + \sqrt{n^2 - \sin^2\theta}} \tag{17}$$

$$r_M = \frac{\sqrt{n^2 - \sin^2\theta} - n^2\cos\theta}{\sqrt{n^2 - \sin^2\theta} + n^2\cos\theta},\ t_M = \frac{2n\ \cos\theta}{\sqrt{n^2 - \sin^2\theta} + n^2\cos\theta} \tag{18}$$

where $n = {}^{n_2}\!/_{n_1}$ the relative refraction index between material 2 and material 1. The equations above, known as the "Fresnel equations", apply for transparent materials.

As described before two cases should be clarified again depending on the relation between n_1 and n_2.

a. $n_1 < n_2$

In this case, both $r_{E,M}$ and $t_{E,M}$ have real values for all incident angles $\theta < \pi/2$. Also t_E and t_M have positive values which means that the refracting transverse waves of electric and magnetic field have the same phase with the respective incident ones. On the other hand the value of r_E is negative for every angle $\theta < \pi/2$, and the value of r_M is: negative for $\theta < \theta_B$, zero for $\theta = \theta_B$, and positive for $\theta_B < \theta < \pi/2$, where θ_B is the Brewster angle ($\tan\theta_B = n = n_2/n_1$). The negative values mean that the respective reflecting waves present a phase difference of π in accordance to the phase of the incident wave. In the special case of $\theta = \theta_B$, there is no reflectance for the transverse magnetic field (!) and when $\theta_B < \theta < \pi/2$ there is no phase difference for it.

b. $n_1 > n_2$

Both $r_{E,M}$ and $t_{E,M}$ have real values but only for incident angles $\theta < \theta_c$, where θ_c is the critical angle for total reflection ($\sin\theta_c = n = n_2/n_1$). For those values of θ, both t_E and t_M as well as r_E are positive indicating that these waves exhibit no phase difference with the respective incident ones. As before the value of r_M depends on the Brewster angle but in a different way, r_M is: positive for $\theta < \theta_B$, zero for $\theta = \theta_B$, and negative for $\theta_B < \theta < \theta_c$. So for the last case a phase difference of π is observed. Finally in the case of $\theta_c < \theta < \pi/2$, for all coefficients the values are complex numbers and the phenomenon of total reflection is observed.

2.4.3 Optical tunneling

The optical tunnelling is an interesting optical phenomenon which can be explained only by considering the light as an electromagnetic wave. This phenomenon arises in the case of total reflection where:

$$\sin\theta \succ \sin\theta_c = n \Rightarrow n^2 - \sin^2\theta \prec 0 \Rightarrow \sqrt{n^2 - \sin^2\theta} = \pm i\sqrt{\sin^2\theta - n^2}$$

By substitution of the negative values in the r_E and r_M relations:

$$r_E = \frac{\cos\theta + i\sqrt{\sin^2\theta - n^2}}{\cos\theta - i\sqrt{\sin^2\theta - n^2}},\ r_M = \frac{n^2\cos\theta + i\sqrt{\sin^2\theta - n^2}}{-n^2\cos\theta + i\sqrt{\sin^2\theta - n^2}} \tag{19}$$

The magnitude of the complex coefficients above equals zero, so they can also be written as: $r_E = e^{i\phi_E}$, $r_M = e^{i\phi_M}$. The arguments φ_E and φ_M can be calculated by the trigonometrical equations:

$$\tan\left(\frac{\varphi_E}{2}\right) = \frac{1}{\cos\theta}\sqrt{\sin^2\theta - n^2} \equiv \tan\beta \ ,\ \tan\left(\frac{\varphi_M}{2} + \frac{\pi}{2}\right) = \frac{1}{n^2}\tan\beta \tag{20}$$

where $0 \prec \beta \prec \pi/2$.

The physical meaning of the relations above is that the amplitudes of the reflected waves of the transverse electric and magnetic fields remain the same. But the reflected wave of the electric field is leading the respective incident wave by a phase of φ_E and the reflecting wave of the magnetic field is following the respective incident wave by a phase of φ_M. Moreover since $|r_E| = |r_M| = 1$, also the $R_E = R_M = 1$ (Eq. 15). This means that during the internal total reflection, the total energy of the incident waves is reflected.

According to the geometric optic, one would expect the reflected wave to arise from the point of the incidence. However in total reflection phenomenon, this is not always the case! The reflected wave appears shifted by a distance z, relatively to the incidence point, known as "Goose–Haenchen shift" as shown in Fig. 2b.(reported in Isaac Newton's works, who could not explain it without Maxwell's equations).

This shift means that part of the incident wave penetrates the material 2 (with $n_2 < n_1$) and moves parallel (z axis) to the boarder surface with an amplitude that is diminishing exponentially as a function of the depth (y axis) in the material 2. This wave is called "evanescent" (Fig. 2a) and is described by the following equations:

$$E_e^E = E_{e0}^E(y)\cos\left(\omega t - k_e z + \varphi_E/2\right) \tag{21}$$

where: $E_{e0}^E(y) = A_e^E e^{-ay}$ and $A_e^E = 2A_i^E \cos\frac{\varphi_E}{2}$ (A_i^E is the amplitude of the incident transverse electric file wave)

$$a = \sqrt{k_1^2 \sin^2\theta - k_2^2} = \frac{2\pi n_2}{\lambda}\sqrt{\left(\frac{n_1}{n_2}\right)^2 \sin^2\theta - 1} \tag{22}$$

$k_e = k_1 \sin\theta$ ($k_1 = n_1 k$, $k_2 = n_2 k$, $k = \frac{2\pi}{\lambda}$, where λ is the wavelength in vacuum)

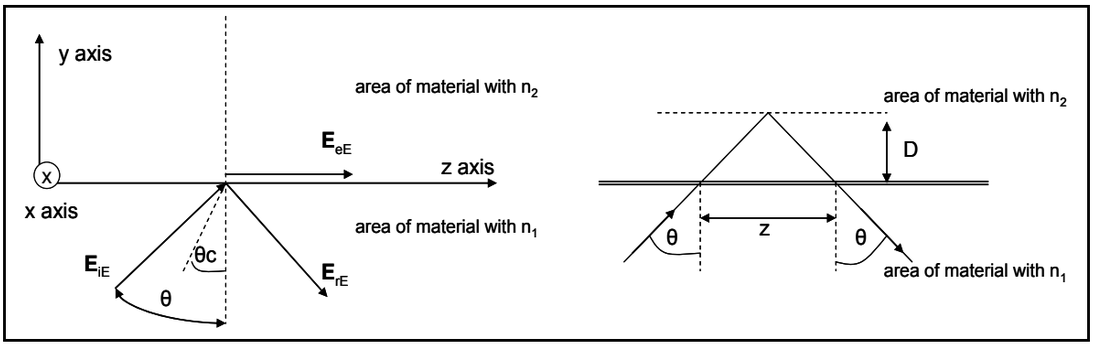

Fig. 2. a) Evanescent wave (Left) and b) Goose–Haenchen shift (right)

The "penetration depth" D, in material 2 is defined as the depth where the amplitude $E_{e0}^E(D) = A_e^E e^{-aD}$ decreases by the factor of e $E_e^E(D) = \frac{A_e^E}{e}$. D is given by:

$$D = \frac{1}{a} = \frac{\frac{\lambda}{2\pi n_2}}{\sqrt{\left(\frac{n_1}{n_2}\right)^2 \sin^2\theta}} \tag{23}$$

By geometry, it is found that the shift of the reflected wave equals: $z = 2D\tan\theta$. In the case of a thin enough layer of material 2 (thickness < D), not all of the evanescent wave rises as a reflected wave. Part of it, propagates through the material 2. In that case the energy of the reflected wave is smaller than the energy of the incident wave and depends on the thickness of material 2. This case, known as optical tunnelling, is one of the effects of the wave nature of light.

2.5 Light Emitting Diodes (LEDs)

Since 1904, these devices have found wide applications in the form of indicator lamps, display elements and sensors. In a junction LED, photons of near-band-gap energy are generated by the process of injection (luminescence or electroluminescence, as described above), in which a large population of electrons, injected into a normally empty conduction

band by forward bias, recombine with holes in the valence band. The device emits light by spontaneous emission. Some of the obvious advantages of the LED as a light source, are simpler fabrication procedures, lower cost, and simpler drive circuitry.
In the case of electroluminescence, the LED converts the input electrical energy into output optical radiation in the visible or infrared portion of the spectrum, depending on the semiconductor material. This conversion takes place in two consecutive events. Initially the energy of carriers in the semiconductor is raised above their equilibrium value by the electrical input energy. Finally most of these carriers, after having lived a mean lifetime in the higher energy state, they give up their energy as spontaneous emission of photons with energy nearly equal to the band gap of the semiconductor. In the case of a doped semiconductor (p- or n- type), the energy of the current carriers can be increased by applying a forward bias to a p-n junction. (Bhattacharya, 1997)
The internal quantum efficiency of the device is defined as the rate of the emission of photons divided by the rate of the supplied electrons. As known, all the injected electrons do not recombine radiatively with holes, leading to an efficiency always less than 100%.
The choice of the proper semiconductor material, depends on the wavelength of the light emission required for a specific application. As expected, lower band gap materials are required for infrared and far-infrared applications while higher band gap materials are required for applications in the visible part of the spectrum. It is important to note that higher band gap materials exhibit higher melting point and lower structural stability. Another important disadvantage of the higher band gap materials is their higher resistivity and the difficulty of being doped. The III-V compounds and especially the binary compounds of GaAs and GaP and the ternary $GaAs_{1-x}P_x$ are considered to be the most important materials for LED's fabrication due to their properties described before.

2.5.1 IR LEDs

For longer wavelengths in the near-infrared region of the spectrum, InP- based compounds are important (i.e. $In_{0.53}Ga_{0.47}As$, $In_xGa_{1-x}P_yAs_{1-y}$). Devices made of these materials operate in the 1.1-1.6 μm range, which overlaps with the spectral region of low loss and minimum dispersion in optical fibers, making them important for applications in optical fiber communication. In general, the use of IR leds offer great advantages in circuit design due to the:

a. low power requirements, making them ideal for personal digital equipment like laptops and telephones
b. low cost and simplicity of circuitry
c. lack of interference with other devices' signals

The advantages they exhibit make them appropriate for applications involving multi-touch screens, based on FTIR technolology. As an example, the designing of single display cockpits (with IR LEDs) is reported by Xalas et al.(2009).
On the other hand there are some design restrictions since signals are wirelessly transmitted. All transmitters and receivers should be almost directly aligned and any blocking material should be avoided. Moreover the transmission length is limited since the performance of such devices drops off by distance. Research is heading for the development of higher power IR LEDs in order to eliminate this problem and as referred, there are already IR LEDs at 940nm with an output power 2.5 times higher than that of a conventional 940 nm LED. (Kitabayashi et al., 2010)

2.5.2 OLEDs

The special case of OLEDs involves the use of organic materials, for example a conducting polymer layer (polyaniline PANI:PSS, Polyethylenedioxythiophene PDOT:PSS) and an emissive polymer layer (Polyohenylenevinylene R-PPV, Polyfluorene PF), between the anode and the cathode of the diode. These devices offer mainly the advantage of different emission colors by synthesizing a variety of chemical structures. Moreover the fabrication cost is less since the vacuum deposition steps required are less and these materials are compatible with printing techniques resulting in low cost for full color applications. The advantages mentioned, led the research to the semiconducting organic materials in order to fabricate electronic devices that are thin, flexible, low cost, and disposable.

The efficiency of an OLED device is defined as the ratio between the electrical power supplied to the device and the optical power that comes out through the glass substrate. It can be divided into the internal efficiency, that is the number of generated photons per injected electron, and the optical outcoupling efficiency which is the percentage of the generated light that is able to escape from the device through the glass substrate. Three factors affect mainly the outcoupling efficiency: a) the refractive index of the emitting material (n = 1.7), b) the refractive index of the substrate (n = 1.5) and c) the reflectivity of the cathode. In a thick device (relative to the wavelength of light), and in absence of scattering effects, the outcoupling efficiency (η) is given by the following analytical formula following from Snell's law:

$$n = \frac{1+R}{2}\left(1-\sqrt{1-\left(\frac{1}{n_e}\right)^2}\right) \tag{24}$$

But in real cases, the thickness of every layer is in the order of the wavelength of the generated light, yielding an angular distribution very different from the isotropic. Therefore, the thickness of every layer and the location of the emitter play also an important role on the angular distribution of the generated photons.

Optimization of OLEDs can be done by enhancing the amount of light that is emitted into air. This can be achieved by optimizing the thickness of the different layers and by inhibiting lateral propagation of the light inside the OLED. The presence of scattering centers in the substrate or especially in the active medium, where most of the light is trapped, could result in an increment of the outcoupling efficiency. Photonic crystals or nanostructured surfaces can also be applied to avoid lateral propagation of the light inside the OLED, bringing more light into the escape cone.

Research about improving the life time and the efficiency seems to be worth it due to the great advantages of OLEDs:

- High efficiency and large area sources.
- High brightness and wide viewing angle.
- Thin, flat and lightweight.
- Low voltage and fast switching technology.
- Form freedom and tunable emission.
- Flexible displays.
- Low cost production.

The great number of OLED applications led to the fabrication of different types according to special needs. Two different classifications can be made according to the matrix type and according to the emission of the OLED. (Andoniadis, 2003)

Matrix type:

a. Passive matrix OLED (PMOLED)
PMOLEDs have strips of cathode, organic layers and strips of anode. The anode strips are arranged perpendicular to the cathode strips. The pixels, emitting light, are formed by the intersections of the cathode and anode. Current is applied by external circuitry to specific strips of anode and cathode, depending on which pixels are chosen to emit light. PMOLEDs are easy to make, but they consume more power than other types of OLED, mainly due to the power needed for the external circuitry. PMOLEDs are most efficient for text and icons and are best suited for small screens such as cell phones, PDAs and, MP3 players. It should be noted that even with the external circuitry, passive-matrix OLEDs consume less battery power than the LCDs that currently power these devices.

b. Active matrix OLED(AMOLED)
AMOLEDs have full layers, instead of strips as PMOLEDs, of cathode, organic molecules and anode. In this case the pixels' matrix is formed by a thin film transistor (TFT) array overlaying the anode. The TFT array itself is the circuitry that determines which pixels get turned on to form an image. Considering that AMOLEDs consume less power than PMOLEDs, since the TFT array requires less power than external circuitry, and that they exhibit faster refresh rates, they are the appropriate choice for large displays such as computer monitors, large-screen TVs and electronic signs or billboards.

OLED emission:

a. Transparent OLED
All the components of the OLED, in this case are transparent (substrate, cathode and anode) and, when turned off, are up to 85 percent as transparent as their substrate. When a transparent OLED display is turned on, it allows light to pass in both directions. A transparent OLED display can be either active- or passive- matrix and can be used for heads-up displays.

b. Top-emitting OLED
In top-emitting OLEDs the substrate is either opaque or reflective and they are more appropriate for active-matrix design. They are usually applied in smart cards.

c. Foldable OLED
In this case the substrates are made of very flexible metallic foils or plastics. Foldable OLEDs are very lightweight and durable. Their use in devices such as cell phones and PDAs can reduce breakage, a major cause for return or repair. Potentially, foldable OLED displays can be attached to fabrics to create "smart" Clothing, with an integrated computer chip, cell phone, GPS receiver and OLED display sewn into it.

d. White OLED
White OLEDs emit white light that is brighter, more uniform and more energy efficient than that emitted by fluorescent lights. Since OLEDs can be made in large sheets, white OLEDs can replace fluorescent lights currently used in homes and buildings resulting in energy saving.

3. Experiment

Simulation is important in proton (or electron) testing because real testing is expensive and it is complicated by the strong dependence of proton damage on energy. The effects of shielding must also be taken into account when this calculation is done, because most of the low energy protons will be removed by even thin amounts of shielding. One important practical difficulty for proton testing is activation of circuits and test boards during irradiation.

We have simulated the damage induced by protons and beta particles of various energies using SRIM-TRIM and CASINO packages respectively. We have modeled an OLED using its cross section (Youtian Tao et al., 2010) which is shown in Table 1.

Layer Name	*Width (Å)*	*Density (g/cm^3)*
Al (aluminum)	1000	2.70
Lithium fluoride	10	2.64
Alq_3 tris(8-hydroxyquinoline) aluminum	300	1.39
BCP(2,9-dimethyl-4,7-diphenyl-1,10-phenanthroline)	100	1.29
NPB (emissive layer) ((1,4-bis(1-naphthylphenylamino)biphenyl)	800	1.326
MoO_3	100	4.69
ITO (indium tin oxide)	1500	7.1

Table 1. Cross Section of an OLED

Before starting the irradiation of the structure above, we performed simulations for protons of various energies on a single layer of aluminum of 1 cm thickness, considering it as a characteristic example of a craft's shield. It was calculated that only protons of energies grater than ~45 MeV could cross over the aluminum layer. Further more it was observed that protons with slightly higher energies than the above mentioned threshold, traverse the shield with residual energy in the MeV range. For example for 50 MeV protons the transmitted ions that emerge from the shield have a mean energy of 11MeV.

In this work protons were simulated with SRIM for the energies of 10keV, 30keV, 100keV, 300keV, 1MeV, 3MeV, 10MeV and 20MeV and around 3million ions considering these values as the protons' energies emerging from a possible shield.

SRIM-TRIM 2010.01 (Stopping and Range of Ions in Matter) can handle ions and neutrons. SRIM 2010.00 calculates the range of ions in the matter (10eV-2GeV/amu) using collisions of ions - atoms. TRIM (Transport of Ions in Matter) accepts up to 8 complex targets from various materials. It calculates the 3D spread of ions as well as the all kinetic phenomena that are related with the loss of their energy: damage of the target, sputtering, ionization and phonons production. With SRIM we obtained the plots of depth versus y-axis, ionization, phonons, collision events, atom distributions and energy to recoils. (Fig. 3, 4).

30keV

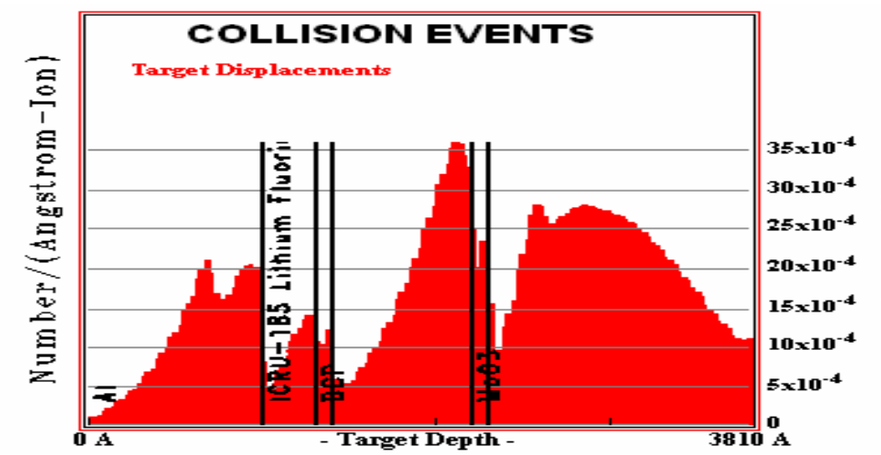

300keV

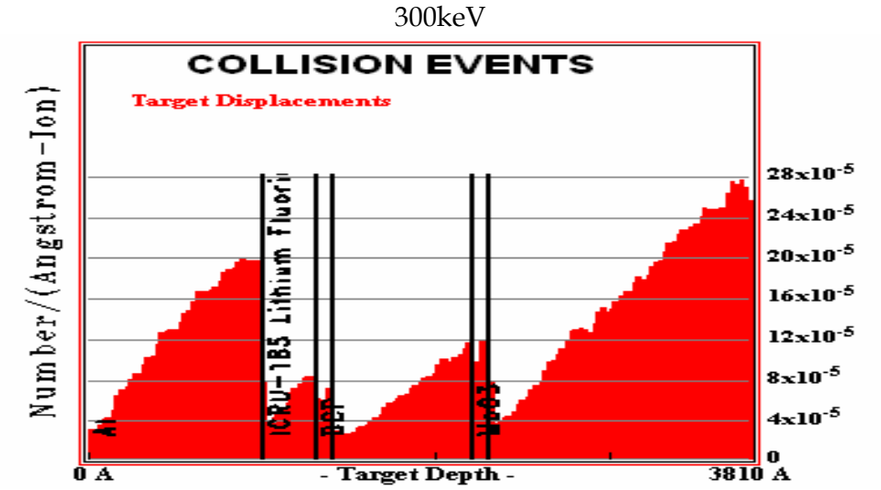

3MeV

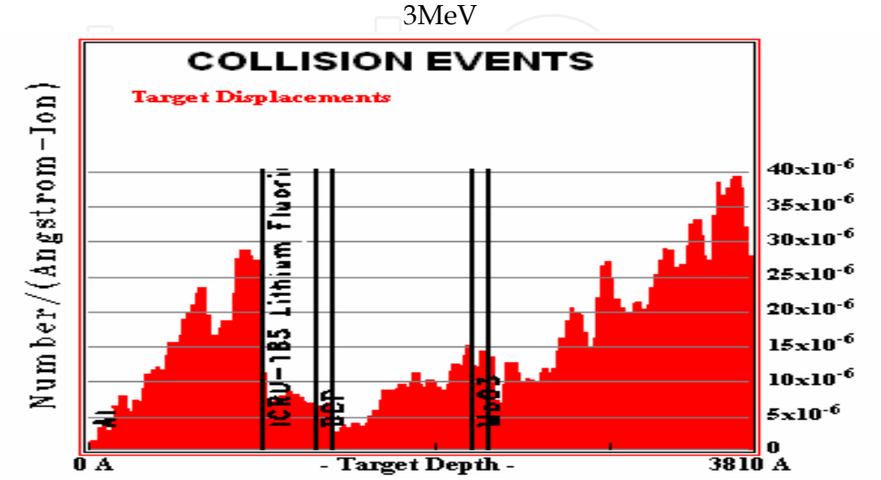

Fig. 3. Displacements distribution across the OLED

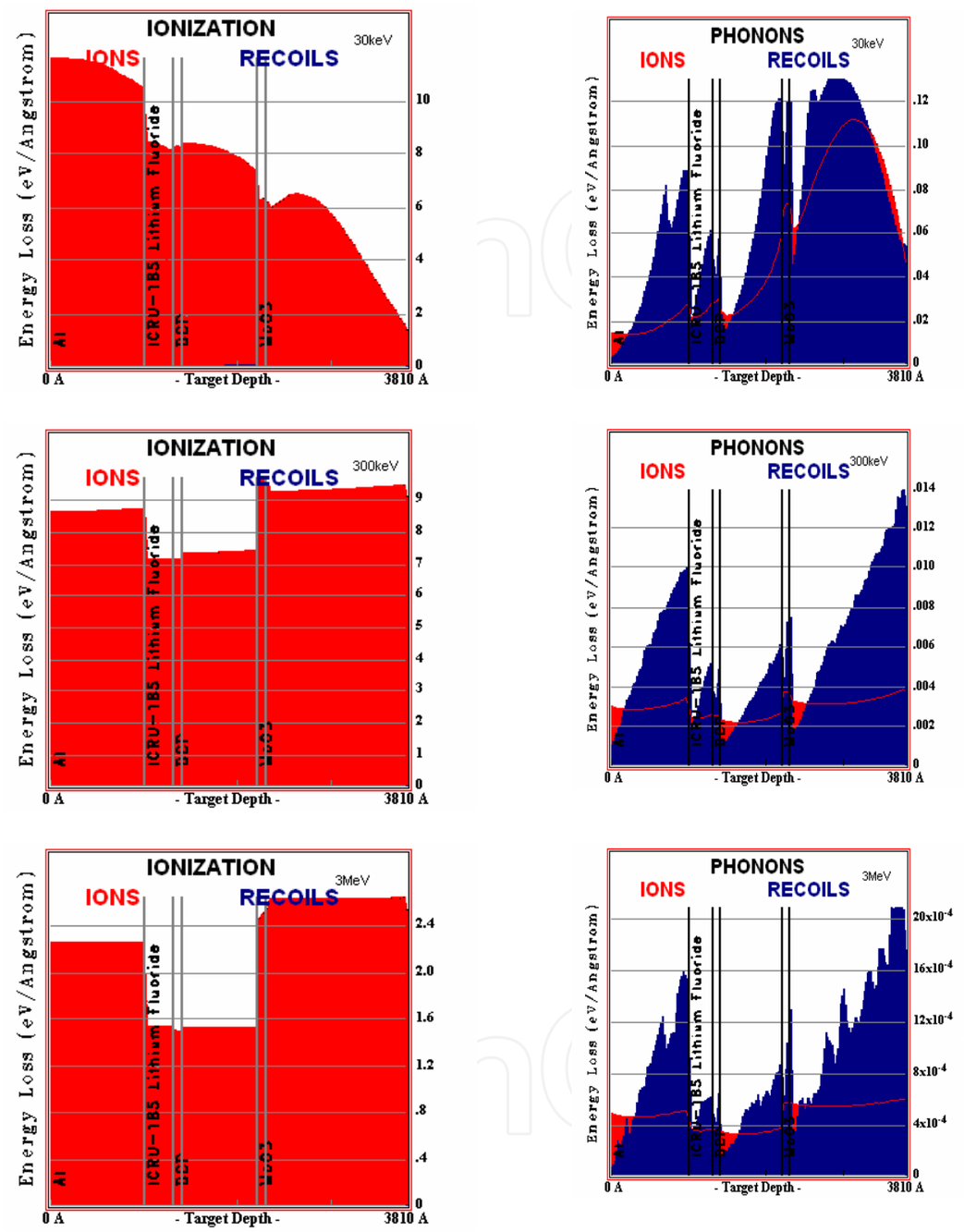

Fig. 4. Ionization (left column) and phonons (right column) distribution across the OLED

Beta particles were simulated with CASINO (Fig.5) with energies ranging from 3 to 30 keV. CASINO v.2.42 (Monte Carlo Simulation of electron trajectories in Solids) is a program with which we can see the trajectories of electrons in the matter as well as their results. When electrons pass through a material, four possible processes may occur: Ionization, Bremsstrahlung, Elastic scattering and nuclear excitation which is usually negligible.

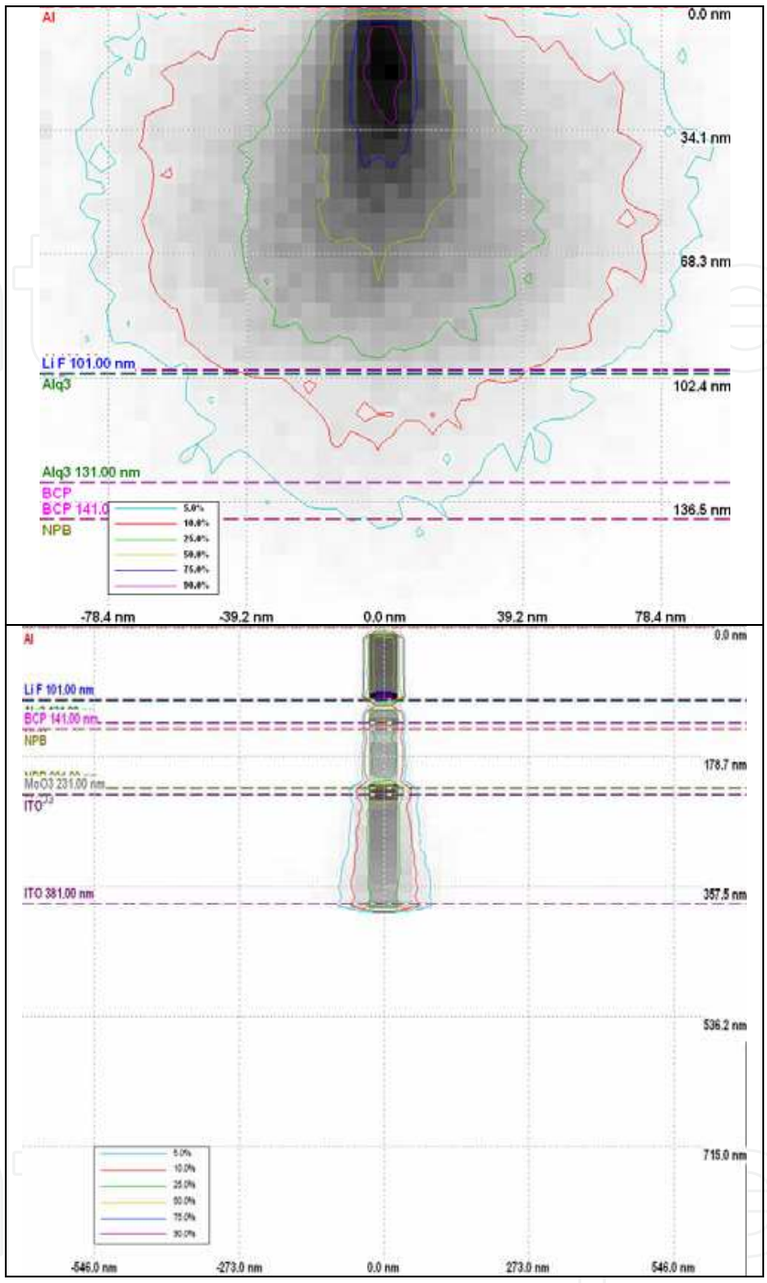

Fig. 5. Typical CASINO output at 3keV(top) and 30keV(bottom)

4. Results and discussion

The main types of radiation effects on materials can be grouped into the following categories:

a. *Impurity Production*: transmutation of nuclei into other nuclei which themselves may be radioactive; this mechanism is from neutrons only through fission and activation. Impurities can also be deposited from the creation of hydrogen or helium when a proton or an alpha particle becomes neutralised in the material of passage.

b. *Atom Displacement* from their normal position in the structure of the material; displacement atoms may leave lattice vacancies and lodge in interstitial locations or cause interchange of dissimilar atoms in the lattice structure.
c. *Ionization*: removal of electrons from atoms in the material and formation of ion pairs in the path of the charged particles.
d. Large *Energy Release* in a small volume, which can result in thermal heating of the material.

By the CASINO energy dispersion graphs it is shown that for energies less than 3keV, the emissive layers of the optoelectronic device remain practically unaffected. Most of the radiation is stopped in the substrate layers affecting their electronic properties. (Fig. 5)

Concerning the TRIM simulations, two major limitations that should be considered are: (a) There is no build-up of ions or damage in the target. Every ion is calculated with the assumption of *zero dose*, i.e. the target is perfect and previous ions have no effect on subsequent ions. (b) The target temperature is 0^{o}K, and there are no thermal effects changing the distribution of ions (thermal diffusion) or affecting the target damage (thermal annealing). Several experiments have been reported at very low temperatures (15-40^{o}K) which validate the TRIM results, but how that thermal effects can be quite substantial. For example, for a low dose of boron ions into crystalline silicon, more than 99% of the target damage anneals at room temperature.

A proton loses energy in small steps through interactions with the electrons in the material. It slows down almost entirely due to Coulomb interactions with the atomic electrons of the target material. Because of the large number of these interactions, the slowing down procedure is nearly continuous and along a straight-line path. As the particle slows down, it captures electron(s) to form a neutral atom and thus has an increased probability to have nuclear collisions that may induce displacements and vacancies in the target material lattice.

The overall behaviour of the OLED studied by SRIM, showed the reduction of ionization, phonons and displacements at higher proton energies justifying the fact that protons of higher energies can interact less with the structure. (Fig. 3, 4)

Moreover phonons produced by ions, exhibit an even distribution across the OLED's layers above 100keV showing no spatial dependence. On the other hand phonons produced by recoils exhibit a distribution similar to the distribution of displacements showing that the formation of displacements is related to the recoil phonons.

All the graphs show less irradiation affects in the emissive layers, which are of main concern in the OLED performance. For that reason we examined in more detail the behaviour of the NPB layer under the protons irradiation. Initially, the phonon dependence on ion energy was examined throughout the OLED after summing the total phonons produced due to ion and due to recoils throughout the device. They were found to follow an exponential decay $phonon = 10^{0.582(ion\ energy)^{-0.900}}$. (Fig. 6)

A similar decay was observed in the NPB emissive layer but with some interesting variations of the exponents. It was calculated that in this layer ion phonons decrease as the recoil phonons do, as the ion energy increases although the amount of recoil phonons dominates at each energy. More specifically $ion\ phonons = 10^{-0.354(ion\ energy)^{-0.887}}$ and $recoil\ phonons = 10^{0.0800(ion\ energy)^{-0.910}}$. (Fig. 7) Similar decay behaviour holds for the ionization distribution where, $ionization\ due\ to\ ions = 10^{2.53(ion\ energy)^{-0.686}}$ and $ionization\ due\ to\ recoils = 10^{-0.164(ion\ energy)^{-0.935}}$. (Fig. 8) These last relations demonstrate that in the emissive layer, ionization from ions dominates the ionization from recoils (~ 3 orders of magnitude) and also that the ionization due to recoils falls off much faster than the one from ions as the energy of the incident protons increases.

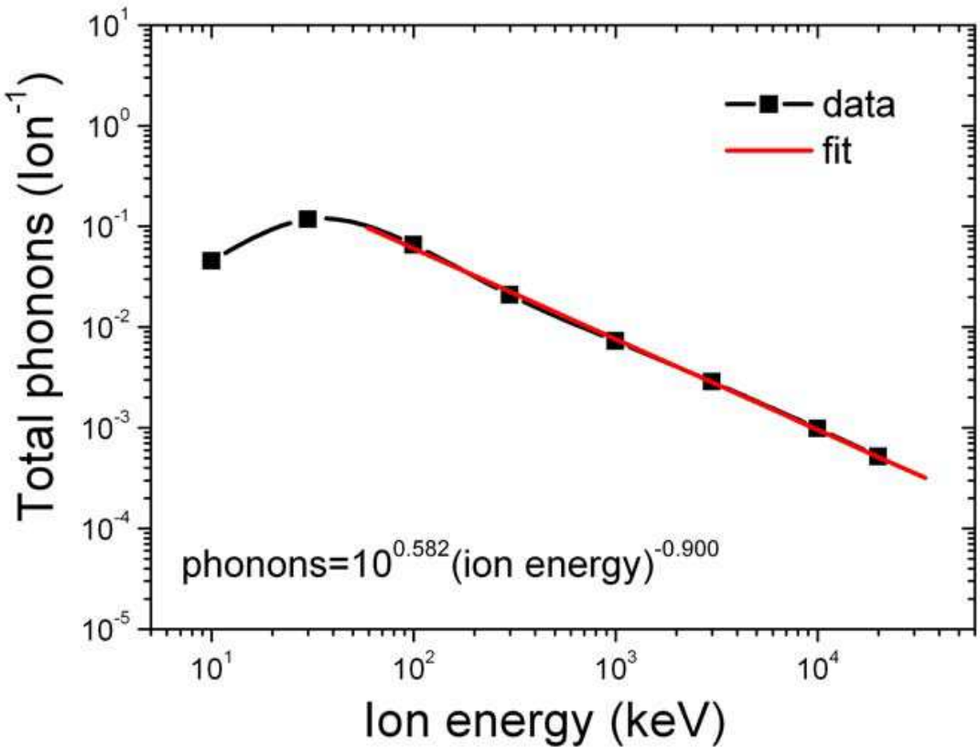

Fig. 6. Total phonons as a function of proton energy

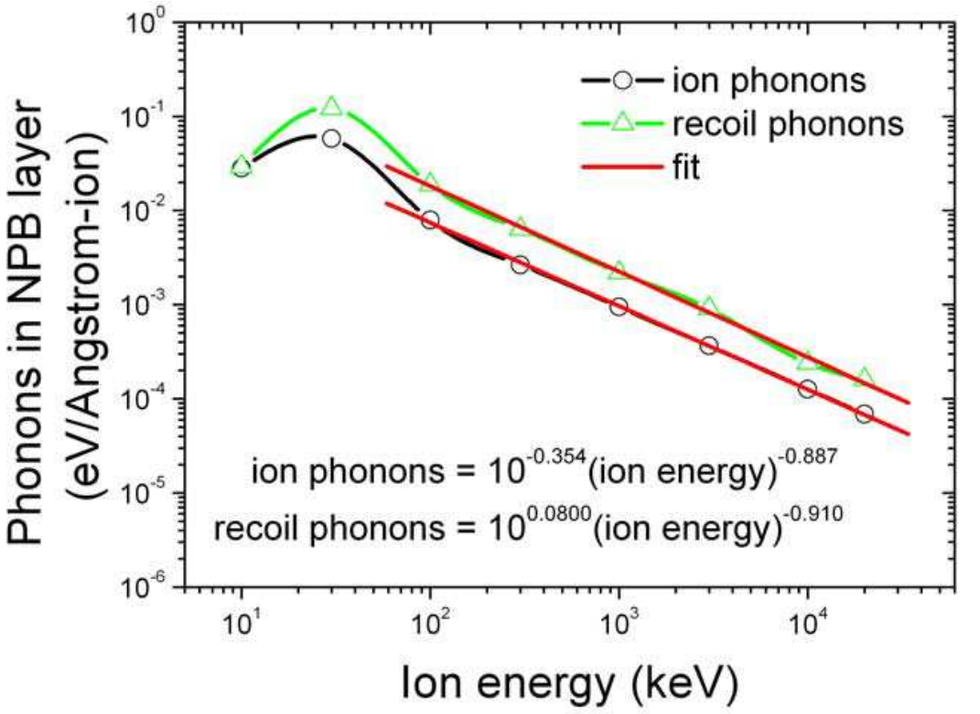

Fig. 7. Phonons generated by protons and recoils in NPB layer

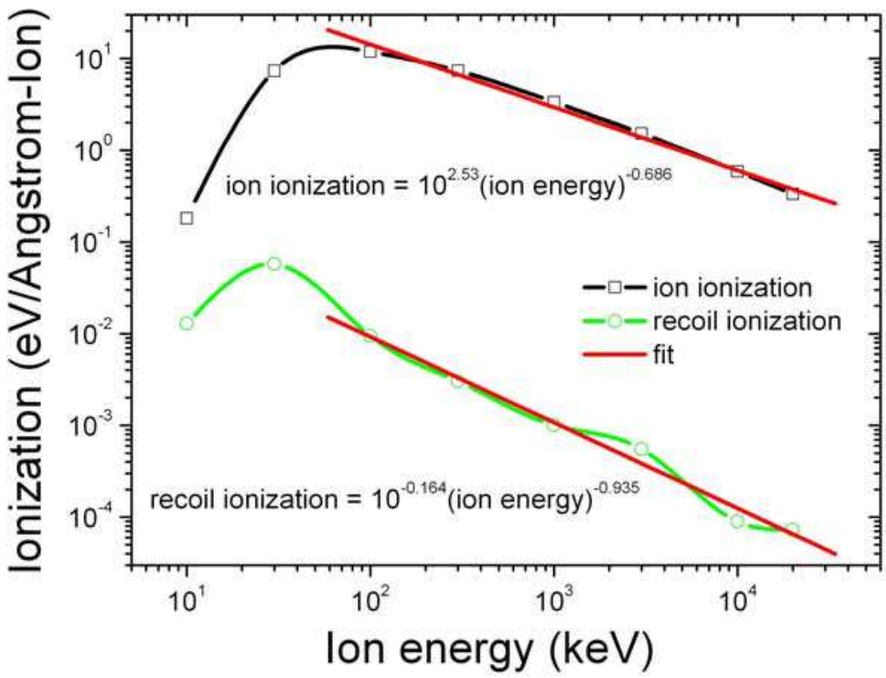

Fig. 8. Ionization generated by protons and recoils in NPB layer

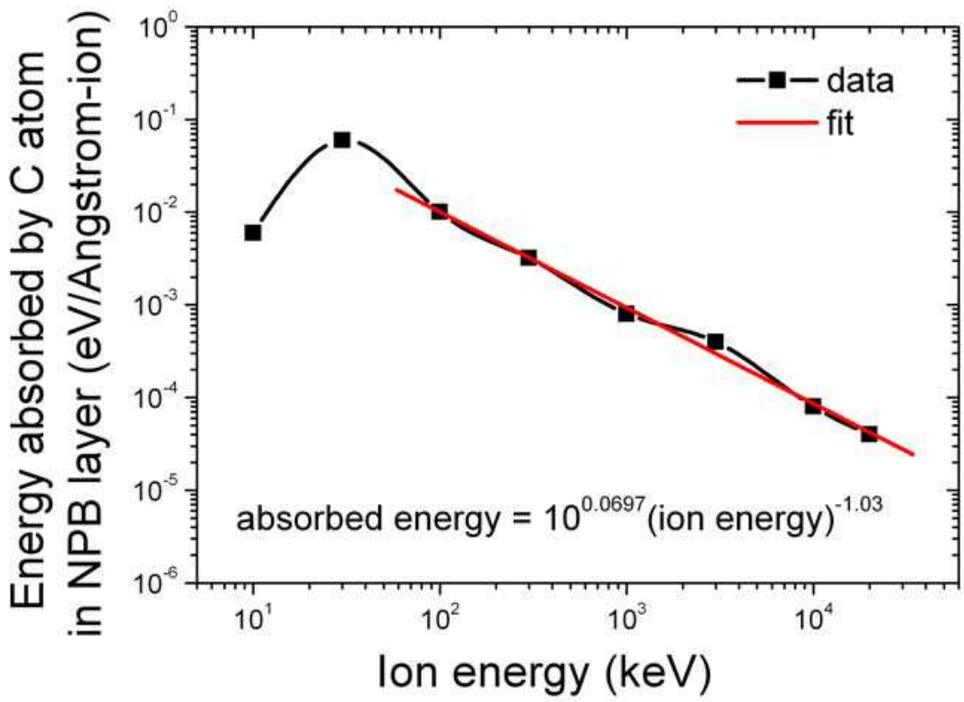

Fig. 9. Energy absorbed by C in NPB layer

By comparing the results for phonons and ionization, one can see that phonons due to ions decrease in a faster manner than the ionization due to ions as the ion energy increases. Considering that phonons are strictly connected to displacements and consequently to the formation of non radiative centres, the above statement indicates the possibility that in the MeV range the electrical behaviour is more affected due to excess of carriers, while the effects seem to be less for the optical behaviour which should be highly affected in the keV range.

Eventually, we studied the behaviour of carbon in the NPB layer since this element exhibited the higher energy absorption in the specific layer. We found a decay behaviour similar to those discussed above for the energy absorption (Fig. 9) and the vacancy formation (Fig. 10) in carbon that is: *energy absorbed*=$10^{0.0697}$*(ion energy)*$^{-1.03}$ and *vacancies*=$10^{-2.02}$*(ion energy)*$^{-0.985}$. Both of them present a dependence onto the ion energy very similar to that of the previous quantities with exception of the ionization due to ions.

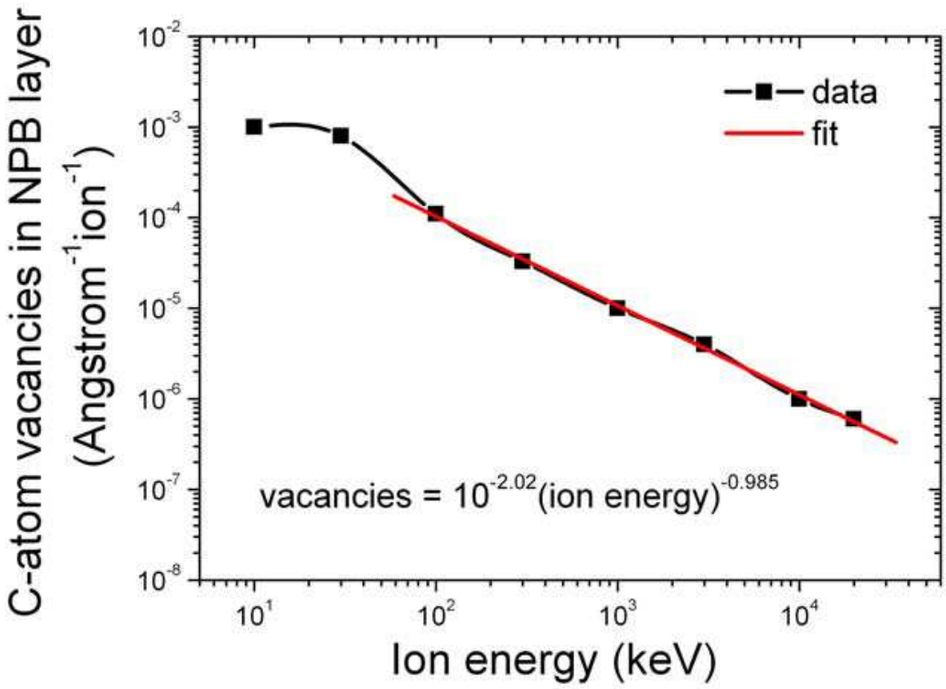

Fig. 10. Vacancies induced in C in NPB layer

5. Conclusions

Simulation of damages induced in optoelectronic devices carried out using SRIM and CASINO packages. The energies used for protons particles were from 10keV to 20MeV. The energies used at CASINO, for b$^-$ particles, were from 3keV to 30keV. We obtained the plots of depth versus y-axis, ionization, phonons, collision events, atom distributions and energy to recoils. Ionizing radiation is proved to affect the layers of the OLED structure simulated, as described above after the analysis of ionization, displacement and phonons induced by proton irradiation. As described before, in the theoretical part, changes in the material

structure, strongly affect its optoelectronic properties and thus the device operation resulting in the whole circuit's malfunction.

We aim to investigate the appropriate elements that can be used in the substrate and in the emissive layers by a specific analysis layer by layer. We also aim to study the neutrons and alpha particles radiation effect.

There are additional permanent damage effects caused by heavy ions. These include microdose damage, and the problem of gate rupture in thin oxides which is less well understood. Recent work (Johnston A.H., 2000) on catastrophic damage in linear circuits shows that this remains a significant problem in space and more work needs to be done.

The optimization of the simulation results together with the modelling of novel devices which will be produced for us in Crete (FORTH) will assist the design of the prototype of a multi-touch screen based on FTIR technology for single display cockpits (IR LEDS) immune to any radiation effects.

It is critical that soft errors (or single event upset (SEU)) (neutrons density increases with height and neutrons with lower energy introduce SEUs) (Psarakis, 2008) which are induced by ionizing radiation must be eliminated from the optoelectronic devices as they are used in the aerospace industry (circuits with high fidelity requirements).

By comparing the effect of ionizing radiation on different material layers and thicknesses, we aim to minimize the operational faults due to structural changes. It should be noted that current research on packaging and device scaling has also improved the performance of ICs.

6. References

Andoniadis H. ,(2003) *Overview of OLED display technology*, OSRAM

Bhattacharya Pallab (1997) Semiconductor Optoelectronic Devices, Prentice Hall, Upper Saddle River, ISBN:0-13-495656-7, New Jersey

Drouin D. , Scanning, 29, Issue 3 , May 2007, 92 – 101

Freudenrich Craig (2004), *How OLEDs Work,*

Johnston A.H., (2000) *4th International Workshop on Radiation Effects on Semiconductor Devices for Space Application*, Tsukuba, Japan, (2000) Radiation Damage of Electronic and Optoelectronic Devices in Space.

Kitabayashi Hiroyuki , Kawabata Yoshisumi , Matsubara Hideki, Miyahara Kenichi and So Tanaka (2010). Development of High Power Infrared LED, *Sei Technical Review*, 70, (April, 2010), 71-74

Papakitsos A., (2002) *Lectures Notes on Applied Optoelectronics*, TEI of Pireaus, Greece.

Psarakis M., (2008) *Lecture Notes on Reliable embedded systems*, University of Piraeus, Greece.

Lin Shih-Yen, Tseng Chi-Che, Lin Wei-Hsun, Mai Shu-Cheng, Wu Shung-Yi, Chen Shu-Han, and Jen-Inn Chyi. (2010). Room-temperature operation type-II GaSb/GaAs quantum-dot infrared light-emitting diode. *Applied Physics Letters*, 96, (March, 2010), ISSN: 0-553-37783-3

Xalas A., Sgouros N., Kouros P., Ellinas J., .(2009). One Display for a Cockpit Interactive Solution, *era-4 Conference Proceedings*, ISSN:1791-1133, Spetses, September 2009, TEI Piraeus, Aigaleo

Yariv Amnon (1976) Introduction to Optical Electronics Holt, Rinehart and Winston, ISBN: 9780030898921, New York

Youtian Tao, Qiang Wang, Liang Ao, Cheng Zhong, Chuluo Yang, Jingui Qin, and Dongge Ma. Highly Efficient Phosphorescent Organic Light-Emitting Diodes Hosted by 1,2,4-Triazole-Cored Triphenylamine Derivatives: Relationship between Structure and Optoelectronic Properties, *J. Phys. Chem*. C, 114, 601–609, (2010)

Ziegler J., Biersack Jochen P., Ziegler Matthias D. (2010). SRIM - The Stopping and Range of Ions in Matter, Lulu Press Co., Morrisville, NC, 27560 USA

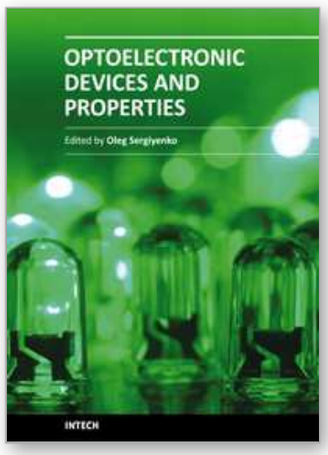

Optoelectronic Devices and Properties

Edited by Prof. Oleg Sergiyenko

ISBN 978-953-307-204-3
Hard cover, 660 pages
Publisher InTech
Published online 19, April, 2011
Published in print edition April, 2011

Optoelectronic devices impact many areas of society, from simple household appliances and multimedia systems to communications, computing, spatial scanning, optical monitoring, 3D measurements and medical instruments. This is the most complete book about optoelectromechanic systems and semiconductor optoelectronic devices; it provides an accessible, well-organized overview of optoelectronic devices and properties that emphasizes basic principles.

INTECH
open science | open minds

InTech Europe
University Campus STeP Ri
Slavka Krautzeka 83/A
51000 Rijeka, Croatia
Phone: +385 (51) 770 447
Fax: +385 (51) 686 166
www.intechopen.com

InTech China
Unit 405, Office Block, Hotel Equatorial Shanghai
No.65, Yan An Road (West), Shanghai, 200040, China
中国上海市延安西路65号上海国际贵都大饭店办公楼405单元
Phone: +86-21-62489820
Fax: +86-21-62489821

IntechOpen